CONDENSED MATTER PHYSICS

Microscopic insights to spin transport–driven ultrafast magnetization dynamics in a Gd/Fe bilayer

Bo Liu, Huijuan Xiao, Martin Weinelt*

Laser-induced spin transport is a key ingredient in ultrafast spin dynamics. However, it remains debated to what extent ultrafast magnetization dynamics generates spin currents and vice versa. We use time- and spin-resolved photoemission spectroscopy to study an antiferromagnetically coupled Gd/Fe bilayer, a prototype system for all-optical switching. Spin transport leads to an ultrafast drop of the spin polarization at the Gd surface, demonstrating angular-momentum transfer over several nanometers. Thereby, Fe acts as spin filter, absorbing spin majority but reflecting spin minority electrons. Spin transport from Gd to Fe was corroborated by an ultrafast increase of the Fe spin polarization in a reversed Fe/Gd bilayer. In contrast, for a pure Gd film, spin transport into the tungsten substrate can be neglected, as spin polarization stays constant. Our results suggest that ultrafast spin transport drives the magnetization dynamics in Gd/Fe and reveal microscopic insights into ultrafast spin dynamics.

INTRODUCTION

Ultrafast manipulation of spins is a central issue of spintronic applications, which aim to realize high-speed and energy-efficient data technologies (*1*). In 3d- and 4f-based magnetic metals, strong out-of-equilibrium dynamics can be driven by femtosecond laser pulses, and the magnetization is altered on a subpicosecond time scale (*2*). After the discovery of ultrafast demagnetization in 3d metals, all-optical switching (AOS) was found particularly in ferrimagnetic 3d-4f materials, whereby the magnetic order is reversed by applying femtosecond laser pulses without an external magnetic field (*3*, *4*). This tremendous development in ultrafast magnetization manipulation proves the high potential for future information technologies, and understanding its microscopic origin is imperative for both fundamental physics and spintronic applications.

It is consensus that ultrafast magnetization dynamics is described by local and nonlocal processes of angular momentum transfer (*5*–*13*). Locally, changes of angular momentum that drive ultrafast demagnetization are attributed to coherent spin transfer (*6*, *14*–*17*) and various spin-flip processes induced by laser excitation, such as electron-electron, electron-magnon, and electron-phonon scatterings (*18*–*21*). In the first process, the laser field coherently excites spin transfer between intersites of the magnetic system. The second process increases scattering rates of various spin-flip events, and the lattice acts as the final sink for the transferred angular momentum in the presence of spin-orbit coupling.

In addition, nonlocal spin transport plays an important role for ultrafast spin dynamics (*22*–*32*). In spin valve structures, transport of spin currents affects the speed and magnitude of the demagnetization process (*28*, *32*). In noncollinear magnetization configuration, spin-wave dynamics can be launched via the spin transfer torque (*26*, *33*, *34*). Although it is experimentally obvious that spin transport is generally accompanied with the ultrafast demagnetization process, there is still no conclusive evidence whether spin currents are generated by the demagnetization process or drive ultrafast demagnetization after laser excitation. The pioneering theoretical description by Battiato *et al.* (*31*) suggested that upon laser pumping, excited spin majority carriers can move out of the probed region faster than spin minority electrons due to spin-dependent lifetimes and velocities of hot electrons. This causes a net superdiffusive spin current flowing out of the ferromagnetic layer, which contributes to the demagnetization. Alternatively, it was argued that the spin current is a consequence of or concomitant to the demagnetization process due to magnon excitation (*35*–*41*). The angular momentum is transferred from the local to the itinerant electrons, which results in a spin current. The latter acts as a bottleneck for the demagnetization process (*38*).

A main challenge to address the microscopic role of spin transport in ultrafast spin dynamics is the simultaneous occurrence of both local and nonlocal angular momentum transfer because the time scale of local spin-flip scatterings and spin transport (tens of femtoseconds) is comparable. In this regard, the contribution of spin transport can only be clearly identified when local spin-flip scattering plays a minor role in ultrafast demagnetization. As demonstrated in a previous report, this conjecture holds for gadolinium where local spin-flip scattering does not change the spin polarization of the Gd surface state but only reduces its exchange splitting in the first 10 ps after laser excitation (*42*).

Therefore, the spin polarization of the Gd surface state is an excellent sensor to study the role of spin transport in ultrafast demagnetization in a Gd-based magnetic heterostructure. Any ultrafast variation in spin polarization must arise from spin transport.

In this letter, we use time- and spin-resolved photoemission spectroscopy to investigate the relationship between spin transport and ultrafast demagnetization in a ferrimagnetic Gd/Fe bilayer epitaxially grown on W(110) (see Fig. 1A). These rare earth/transition metal bilayers are prototype systems to achieve AOS (*43*, *44*). In comparison to all-optical methods that provide momentum- and energy-averaged information from multiple layers or interfaces, photoemission spectroscopy is surface sensitive and state selective. Using spin- and time-resolved photoemission, transient exchange splitting and spin polarization can be directly monitored (*13*, *23*, *42*, *45*, *46*). Our findings suggest that ultrafast spin transport dominates the demagnetization process in a ferrimagnetic Gd/Fe bilayer

Fachbereich Physik, Freie Universität Berlin, Arnimallee 14, 14195 Berlin, Germany.
*Corresponding author. Email: weinelt@physik.fu-berlin.de

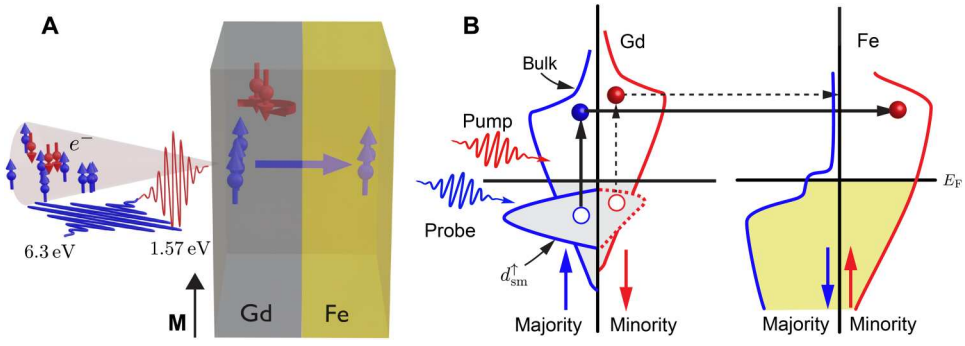

Fig. 1. Ultrafast spin transport in a ferrimagnetic Gd/Fe bilayer after femtosecond excitation probed by time- and spin-resolved photoemission of the Gd surface state. (**A**) Gd and Fe are excited by an infrared (IR) pump pulse ($h\nu$ ~ 1.57 eV) that generates hot electrons. The transient spin polarization and binding energy of the Gd $d^{\uparrow}_{sm}$ surface state (occupied, spin-mixed component) are probed by a time-delayed ultraviolet (UV) pulse ($h\nu$ ~ 6.3 eV). (**B**) Schematic spin-resolved density of states of Fe and Gd for a Gd/Fe bilayer on W(110). Because of the opposite in-plane magnetization of the Fe and Gd layers, majority spin electrons in Gd (blue) become minority spin electrons in Fe and vice versa for spin minority electrons (red). The IR pump pulse excites electrons from the Gd $d^{\uparrow}_{sm}$ surface state into Gd bulk states (OISTR). While spin majority electrons are transported into the Fe layer as indicated by the thick arrow, the transfer of spin minority electrons is minor (dashed thin arrow). The spin-dependent density of states of Fe acts as a spin filter (*65*, *66*). This leads to an ultrafast drop of the Gd spin polarization probed at the Gd surface. The spin-mixed occupied surface state $d^{\uparrow}_{sm}$ of Gd shows an apparent peak splitting induced by the antiparallel aligned Fe magnetization.

rather than local spin-flip scattering mediated by spin-orbit coupling. In the bilayer, we find that after optical excitation, the occupied majority part (↑) of the spin-mixed (sm) surface state of Gd (denoted as $d^{\uparrow}_{sm}$) shows an ultrafast decrease of its spin polarization by 20% within the first ~100 fs. Upon quenching of the spin polarization, this process is partially counteracted by an ultrafast increase of the $d^{\uparrow}_{sm}$ binding energy. In contrast, the pure Gd/W(110) film shows a constant spin polarization and a shift to lower binding energy of the occupied $d^{\uparrow}_{sm}$ surface state upon optical excitation. Moreover, for the Gd/Fe bilayer system, the transient electronic temperature rapidly decays to its initial value within 1 ps. Hot carriers must be efficiently transported out of the Gd layer and absorbed in the Fe layer before they can heat the lattice, while in pure Gd/W(110), electron and phonon subsystems equilibrate at an elevated temperature. This spin transport from Gd to Fe was corroborated by an ultrafast increase of the Fe spin polarization in a reversed Fe/Gd bilayer. Thus, the decay of spin polarization at the surface of the Gd/Fe bilayer is consistently attributed to spin transport.

The relevant microscopic process is illustrated in Fig. 1B. Electrons in the occupied $d^{\uparrow}_{sm}$ Gd surface state, which we use as spin-polarized sensor, are photoexcited to unoccupied bulk states by the infrared pump pulse. This corresponds to an optical-induced transfer of both majority and minority spins from surface to bulk states. Because the in-plane magnetizations of the Gd and Fe layers are antiparallel aligned, majority spin electrons in Gd become minority spin electrons in Fe and vice versa. Exchange splitting and the concomitant spin-dependent density of states in Fe favor the transport of laser-excited Gd majority spin electrons into the Fe layer. The laser-triggered electron transport happens within 100 fs and leads to a drop of the Gd spin polarization because the Fe layer acts as a spin filter. We record this change in spin polarization by photoemission of the Gd $d^{\uparrow}_{sm}$ surface state with an ultraviolet (UV) probe pulse.

RESULTS

For the further discussion and interpretation of results, it is imperative to know the electronic structure of the Gd surface state. The d_{z^2} surface state of Gd is exchange split into an occupied and an unoccupied part below and above the Fermi level E_F. For temperature $T \rightarrow 0$ K, they correspond to the pure spin majority $d^{\uparrow}_{z^2}$ and spin minority $d^{\downarrow}_{z^2}$ surface bands, respectively. We note that we observe only the occupied (majority spin) part of the surface state, denoted as $d^{\uparrow}_{sm}$. It was shown in pump-probe photoemission spectroscopy that the unoccupied part of the surface state has a three orders of magnitude lower count rate than its occupied counterpart (*47*). Therefore, we do not observe the unoccupied surface state in our spin- and time-resolved photoemission experiment. However, for a finite temperature, the surface and valence states of Gd are known to show spin mixing (*48*, *49*). Spin mixing or band mirroring is usually related to the excitation of magnons at finite temperatures. In other words, the spin polarization of the valence and surface bands, corresponding to their magnetic moment, fluctuates in time and space. With our photoemission measurement, we average over these fluctuations and observe a reduced spin polarization. Thus, already, the occupied part of the Gd surface state $d^{\uparrow}_{sm}$ shows both majority and minority spin components.

Figure 2 (A and B) compares spin-resolved photoemission data of the Gd $d^{\uparrow}_{sm}$ surface state as a function of pump-probe delay for a Gd/Fe bilayer and a pure Gd layer, respectively. The initial sample temperature was 100 K. This is far below the compensation temperature of the Gd/Fe bilayer of ~285 K (see the Supplementary Materials) and allows us to compare the spin dynamics in both Gd samples avoiding AOS. The up (blue) and down (red) triangles represent the spin majority and spin minority components of the occupied $d^{\uparrow}_{sm}$ surface state for both samples. The solid line is a fit to the data according to Eq. 1 (see Materials and Methods). It consists of a Lorentzian to describe the minority or majority spin components of the $d^{\uparrow}_{sm}$ surface state on top of a linearly increasing background. The occupied $d^{\uparrow}_{sm}$ surface state is cut by the Fermi function, and spectra are convolved with a Gaussian accounting for the energy resolution

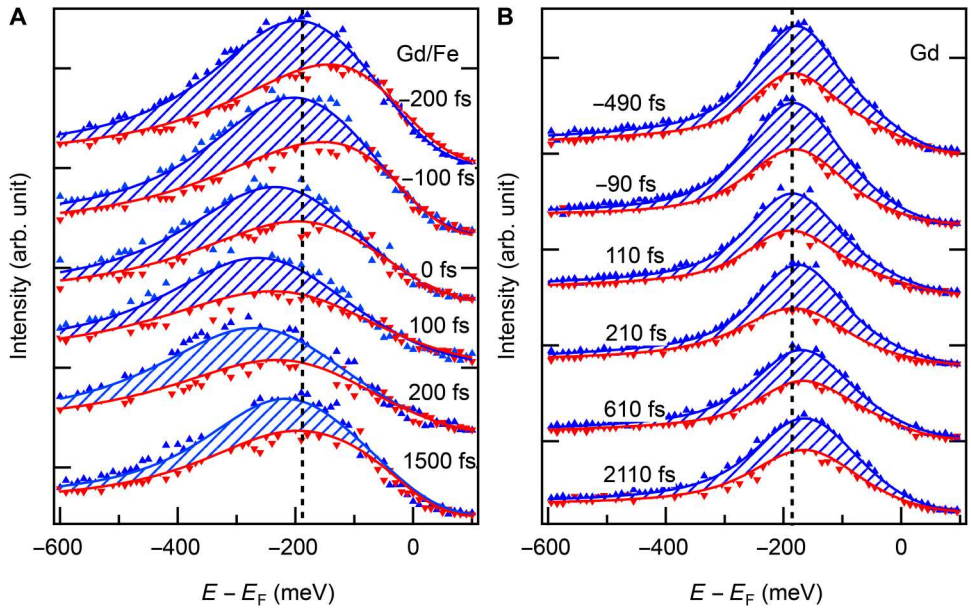

Fig. 2. Spin-resolved spectra of the Gd surface state. (**A**) Spin majority (blue up-triangle) and spin minority (red down-triangle) components of the occupied, spin-mixed Gd surface state $d^{\downarrow}_{sm}$ for the Gd/Fe bilayer before (negative delay) and after optical excitation. Note the peak splitting between both components induced by the spin-dependent hybridization of Fe and Gd bands. The initial peak position of the majority component of the surface state is indicated by the dashed line. The surface state moves first away from E_F and then shifts back. (**B**) Spin-resolved majority and minority components of the $d^{\downarrow}_{sm}$ surface state for a pure Gd film on W(110) at various pump-probe delays. The surface state peak shows the expected behavior. It moves toward E_F after optical excitation, indicating a drop of the exchange splitting. Solid lines correspond to fits according to Eq. 1.

of the experiment. The black dashed vertical lines in Fig. 2 mark the peak maximum of the majority component of the Gd surface state before optical excitation.

We first analyze the binding energy E_B (defined by the respective peak maximum) of the $d^{\uparrow}_{sm}$ surface state and its dynamics. The respective peak positions of majority and minority spin components are summarized in Fig. 3. Already, the binding energy reveals clear differences between the Gd/Fe bilayer and the pure Gd layer. Before optical excitation (at negative pump-probe delay), the spin-mixed occupied surface state in the Gd/Fe bilayer displays a peak splitting of ~80 meV (Fig. 3A) determined from the difference of the spin-dependent peak maxima of ~100 and ~180 meV for spin minority and majority components, respectively (Fig. 3C). These different peak positions and apparent peak splitting are attributed to the coupling between the antiferromagnetically aligned Gd and Fe films, as will be further addressed in Discussion. No such peak splitting is observed in Fig. 3B for the pure Gd film, which shows, as expected, equal E_B of ~180 meV for both spin components (Fig. 3D).

Upon optical excitation, the occupied surface state of the Gd/Fe bilayer (Fig. 3C) shifts within 100 fs to higher E_B. The shift is observed for both the majority and minority spin components of $d^{\uparrow}_{sm}$albeit with a larger amplitude for the latter (70 meV versus 100 meV), which leads to an overall drop of the peak splitting. The overall downshift to higher E_B is unexpected, as it must include a repopulation of the $d^{\uparrow}_{sm}$ surface state (which is cut by the Fermi level) and may indicate an increase of the exchange splitting between occupied $d^{\uparrow}_{sm}$ majority part and unoccupied $d^{\downarrow}_{sm}$ minority part (not detected here) of the surface state. In contrast, for the pure Gd layer, the surface state shifts to lower binding energy by about 20 meV with a time constant of 600 ± 100 fs. Such an upward shift is expected from measurements in thermal equilibrium where the $d^{\uparrow}_{sm}$ surface state shifts to lower E_B with increasing temperature, and the exchange splitting between the occupied and unoccupied components, $d^{\uparrow}_{sm}$ and $d^{\downarrow}_{sm}$, decreases (*48*, *49*). The opposite spectral shift for bilayer and single layer suggests that different microscopic processes must drive spin and electron dynamics in both systems. We note that the applied pump fluence in our experiments was kept the same for both samples (2.3 mJ/cm^2), confirmed by similar maximal electron temperatures of 1010 and 1080 K for Gd and Gd/Fe, respectively.

Second, we consider the spin polarization and population dynamics of the Gd $d^{\uparrow}_{sm}$ surface state. We evaluated the spin polarization of the surface state by integrating in the range of the hatched peak area in Fig. 2 (A and B) over energies $E - E_F$ between −600 and 100 meV. This avoids possible variations of the area due to the spectral shift after optical excitation and therefore reflects most clearly the spin dynamics of the surface state. The integrated intensity of majority and minority spin components I_{maj} and I_{min} is summarized in Fig. 4 (A and B). The spin polarization P of the $d^{\uparrow}_{sm}$surface state is calculated via $P = (I_{maj} - I_{min})/(I_{maj} + I_{min})$ and normalized to $P = 1$ at negative delays. The result is shown in Fig. 4 (C and D) for the Gd/Fe bilayer and the pure Gd layer, respectively. Within the first 100 fs after optical excitation, the spin polarization of $d^{\uparrow}_{sm}$ for the Gd/Fe bilayer is reduced by about 20%, followed by a slower picosecond decrease to $P = 0.75$ at a delay of 1.5 ps. The decay of P is caused by a stronger depopulation of the majority than the minority spin component (Fig. 4A). We observe likewise an ultrafast depopulation of the surface state (within the 86-fs cross-correlation of pump and probe pulses) for the pure Gd film upon optical excitation (Fig. 4B). However, the drop in intensity is

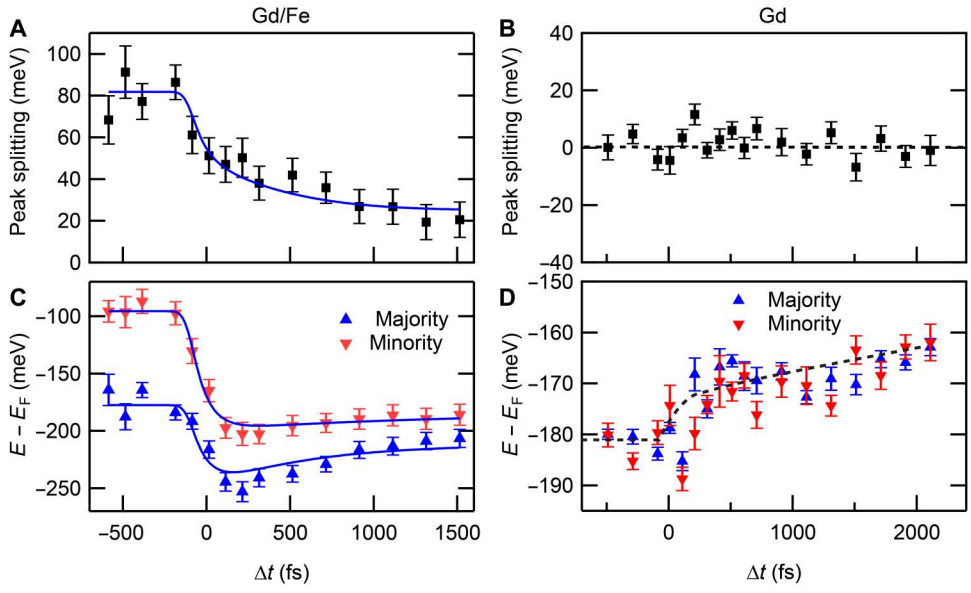

Fig. 3. Dynamics of apparent peak splitting and binding energy. The shift of the peak maximum between the two spin components of the spin-mixed Gd $d^{\uparrow}_{sm}$ surface state in the Gd/Fe bilayer (**A**) and the pure Gd film (**B**). For the bilayer, an initial peak splitting of about 80 meV is induced by the antiparallel magnetized Fe layer. Upon optical excitation, the peak splitting shows a double-exponential decay with a fast 100-fs drop, followed by a slower picosecond decrease. No peak splitting is observed for the pure Gd film. The transient binding energy of the two spin components is shown for the bilayer in (**C**) and for the pure Gd film in (**D**). For the bilayer (C), binding energies of both spin components increase within 100 fs after optical excitation, followed by a slower recovery on the picosecond time scale. For pure Gd (D), binding energies of both spin components of $d^{\uparrow}_{sm}$ decrease with equal amplitude. Blue solid lines are fits to the data according to Eq. 2; dashed lines are guides to the eye.

spin independent, and thus, the spin polarization of the $d^{\uparrow}_{sm}$surface state stays constant (Fig. 4D).

For the Gd/Fe bilayer, both the depopulation and the change in spin polarization of the surface state lead to a drop of the surface magnetization $\mu_s \sim (I_{maj} - I_{min})$. In contrast, for pure Gd based on the equal drop of I_{maj} and I_{min}, the spin polarization P of the occupied surface state $d^{\uparrow}_{sm}$is not altered, and only its depopulation contributes to a change of μ_s. This implies, in particular, that local spin-flip scattering in the Gd layer (of Gd/W and Gd/Fe/W), e.g., via electron-phonon scattering (*20*), does not contribute to a decrease of the spin polarization. Therefore, we attribute the difference between the Gd/Fe bilayer and the pure Gd layer to a nonlocal process, i.e., spin-dependent transport.

The infrared pump laser excites electrons from the occupied surface state into bulk states. This optical excitation process is spin conserving and constitutes an optically induced intersite spin transfer (OISTR) between surface and bulk states. As illustrated in Fig. 1A, the excited carriers from the Gd surface state are transported within the pump-pulse duration of ~40 fs with ballistic or superdiffusive velocity (the Fermi velocity $v_F \sim 10^6$ m/s corresponds to 1 nm/fs) into the bulk toward the adjacent Fe layer. For the Gd/W(110) interface, there is no spin-dependent barrier, and both majority and minority spin carriers are equally transported into the substrate. For the Gd/Fe bilayer, the Fe layer acts as a spin filter. As illustrated in Fig. 1B, the exchange splitting of Fe leads to a much larger density of unoccupied minority spin states above the Fermi level. This favors the transport of excited Gd majority spin electrons into the antiferromagnetically coupled Fe layer, while Gd minority spin electrons are back-scattered at the Gd/Fe interface. The resulting net spin current must lead to a drop of the spin polarization in the Gd layer, which is probed in our spin-resolved photoemission experiment via the Gd surface state.

Figure 4A shows that for the Gd/Fe bilayer, both spin majority (blue up-triangle) and spin minority (red down-triangle) electrons of the Gd surface state are excited by the femtosecond pump pulse, but the spin majority component has a larger depopulation (illustrated by thick and dashed thin vertical arrows in Fig. 1B). In contrast, the pure Gd layer shows similar excitation efficiencies for both spin components (in Fig. 4B) and, thus, a constant spin polarization (Fig. 4D, dashed horizontal line). As will be addressed in more detail in Discussion, we attribute this difference between Gd/W and Gd/Fe/W to the combination of OISTR and spin currents, which occur on similar time scales but are only present in the Gd/Fe bilayer.

The difference in spin transport is also corroborated by the transient electronic temperature T_e in the Gd layer. Figure 5 compares the Gd electronic temperature in both samples. Data points have been extracted from the fit applying Eq. 1 to the data in Fig. 2 (solid lines). As already stated, we reach similar maximum electron temperatures for both samples, indicating comparable absorbed pump fluence. However, the transient electronic temperature decays more rapidly in the Gd/Fe bilayer (black squares) than in the pure Gd layer (red circles). At a pump-probe delay of 1.5 ps, the electronic temperature in the bilayer reaches the base temperature of 100 K, while it stabilizes in the pure Gd layer at around $T_e = T_{lattice} = 350$ K. This further demonstrates that the excited hot electrons in the Gd/Fe bilayer are rapidly removed from the Gd surface because they would otherwise heat the lattice subsystem via electron-phonon scattering. Carrier transport must be less efficient across the Gd/W interface because in the Gd, single-layer electron and phonon subsystems equilibrate at an elevated temperature (*42*).

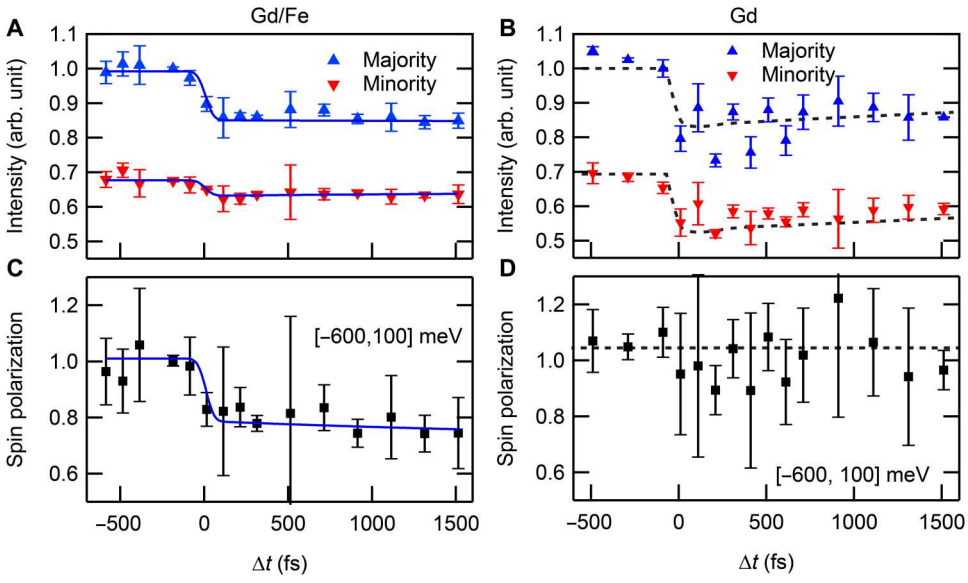

Fig. 4. Transient spectral intensity and spin polarization. (**A** and **B**) Spectral intensity of both spin majority and spin minority components (I_{maj} and I_{min}) of the spin-mixed Gd $d^{\downarrow}_{sm}$ surface state for the Gd/Fe bilayer and the pure Gd film, respectively. To evaluate the peak area, the integration limits were set to $E - E_F = -600$ and 100 meV. (A) For the Gd/Fe bilayer, the peak area of the spin-majority component decreases about two times stronger than that of the spin-minority component upon optical excitation. Blue solid lines are fits to the data according to Eq.2. (B) For the pure Gd film, the integrated peak area of both spin components decreases equally as indicated by the two identical dashed lines. (**C** and **D**) Resulting spin polarization P in the integrated range of the Gd/Fe bilayer and the pure Gd film, respectively. Error bars represent 1 SD. (**C**) For Gd/Fe, the spin polarization shows an instantaneous decrease of about 20% within the pump-probe cross-correlation followed by a slower picosecond decrease. The solid line is derived from the fits in (A) by evaluating the spin polarization P as explained in the main text. (D) For the surface state of the pure Gd layer, the spin polarization remains constant within experimental error bars illustrated by the dashed line. The different transient spin polarization observed for bilayer and single layer demonstrates that the adjacent Fe layer plays a crucial role for ultrafast spin dynamics.

In an attempt to further corroborate the spin transport from the Gd to the Fe layer, we have reversed the layer order and prepared an Fe/Gd/W(110) bilayer (see Materials and Methods). In a recent static photoemission study with a 6.3-eV laser pulse, we have identified an occupied spin-mixed surface resonance $SR^{\downarrow}_{sm}$ with spin minority character on Fe/W(110) (*50*). We now used this resonance of the body-centered cubic (bcc) Fe(110) surface to study spin transport in the reversed bilayer via time-resolved photoemission with 1.57-eV pump and 6.3-eV probe pulses. Figure 6A shows spectra of $SR^{\downarrow}_{sm}$ on Fe/Gd/W(110) for three exemplary pump-probe delays, at −200 fs before excitation, at −50 fs (within the cross-correlation of pump and probe pulses), and at 200 fs after optical excitation. We applied a pump fluence of 4.6 mJ/cm^2, leading to an electron temperature of T_e~ 1300 K (see the Supplementary Materials).

The spectra of the Fe surface resonance $SR^{\downarrow}_{sm}$ confirm the peak shift observed for the Gd $d^{\uparrow}_{sm}$ surface state. The magnetization of Fe and Gd are antiparallel aligned because majority spin electrons in Gd hybridize with minority spin electrons in Fe and vice versa. Accordingly, the minority spin component of the spin-mixed Fe surface-resonance $SR^{\downarrow}_{sm}$ shows a higher binding energy than its majority spin component. While the order is reversed as compared to the Gd $d^{\uparrow}_{sm}$ surface state, the size of the peak splitting of ~80 meV is comparable for Fe $SR^{\downarrow}_{sm}$ and Gd $d^{\uparrow}_{sm}$.

We determined the spin polarization P of the Fe surface resonance by integrating the spectra in Fig. 6A over an energy range from $E - E_F = -780$ to 200 meV. The result is depicted in Fig. 6B. When following the transient spin polarization of the Fe minority spin surface resonance $SR^{\downarrow}_{sm}$, we find a small but clear and reproducible ultrafast increase (!) of P upon optical excitation followed by a decay with a time constant of ~500 fs. We confirmed this ultrafast increase of the spin polarization for Fe layers with thickness of 2 and 5 nm (see the Supplementary Materials).

In other words, before the optical-driven demagnetization of Fe, i.e., the decay of P, the number of minority spin electrons increases. Assuming that the Fe minority spin surface state represents the Fe bulk spin polarization, this indicates transfer of Gd majority spin electrons into the Fe layer, where they become minority spin electrons (cf. Fig. 1B). In contrast, for pure Fe/W(110), the spin polarization simply decreases upon optical excitation, which was attributed to the generation of magnons (*51*).

DISCUSSION

We first recall that our photoemission experiment probes the magnetization dynamics at the surface of the bilayer system. The spin polarization and peak shift of $d^{\uparrow}_{sm}$ for Gd/Fe drop within ~100 fs, while the spin polarization of $SR^{\downarrow}_{sm}$ for Fe/Gd decays with a much larger time constant of ~500 fs. Given the different decay constants and pump fluences (2.3 versus 4.6 mJ/cm^2 for Gd/Fe and Fe/Gd, respectively), it seems appropriate to assume that the dynamics of the Gd layer in Gd/Fe is a little affected by the demagnetization of the Fe layer below.

We have already attributed the difference in spin dynamics between the Gd/Fe bilayer and the pure Gd layer to ultrafast spin transport. Let us first recapitulate the spin dynamics in the pure Gd layer following (*42*, *47*, *52*–*54*). Without spin transport, a

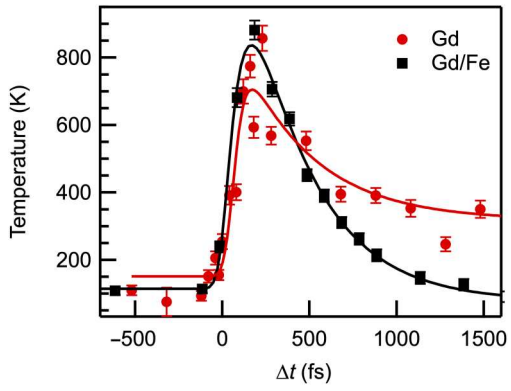

Fig. 5. Transient electron temperature. For Gd/Fe (black squares), the electron temperature T_e decays to its initial values within ~1.5 ps after optical excitation. In the same time interval, the transient temperature reaches ~350 K for the pure Gd film (red circles) and stays well above the initial measurement temperature of 100 K. In the latter case, heat is transported to the lattice. This suggests that spin transport dominates ultrafast demagnetization in Gd/Fe, while phonon-mediated spin-flip scattering dominates demagnetization in pure Gd and leads to the different response of exchange splitting (Fig. 3) and spin polarization (Fig. 4) in bilayer and single layer, respectively. Solid lines are fits to the data according to Eq. 2.

quenching of magnetic moments has to be realized through local spin-flip scattering (*20*), and the lattice subsystem acts as a final sink for the angular momentum (*5*). For Gd on W(110), the spin polarization P of the $d^{\uparrow}_{sm}$ surface state does not change after ultrafast optical excitation. This means that local scattering of the hot valence electrons with phonons, magnons, or electrons (*20*, *55*) does not change the spin polarization (*56*, *57*). Still, we observe OISTR from surface to bulk states, which leads to an equal depopulation of both the majority and minority spin components of the occupied $d^{\uparrow}_{sm}$ surface state by about 20%. This leaves the spin polarization constant $P^{exc} = (0.8\, I_{maj} - 0.8\, I_{min})/(0.8\, I_{maj} + 0.8\, I_{min}) = P$ but contributes to demagnetization of the Gd surface $\mu_s^{exc} \sim (0.8\, I_{maj} - 0.8\, I_{min}) = 0.8\, \mu_s$. This is in line with the ultrafast drop of the surface-sensitive magnetic second harmonic signal reported in (*47*, *54*). During electron-phonon equilibration, the occupied surface state $d^{\uparrow}_{sm}$ shifts toward E_F. This indicates a drop of the exchange splitting of the d_{z^2} surface state because the unoccupied minority part $d^{\uparrow}_{sm}$ shows a nearly constant binding energy (*47*). The observed time constant of 600 fs for this upward shift is comparable to the drop of the exchange splitting observed for Gd bulk in (*52*) and attributed to electron-phonon scattering.

We now turn to the spin dynamics in the Gd/Fe and Fe/Gd bilayers on W(110). For Gd/Fe, we observe a spin-dependent depopulation and a concomitant drop of both spin polarization and surface magnetization. As already mentioned, the Fe layer must act as a spin filter. In the bilayer, the magnetization of Gd and Fe are antiparallel aligned. Thus, Fe with a higher fraction of unoccupied minority spin states favors transport of Gd majority spin electrons across the Gd/Fe interface into the Fe layer where they become minority spin carriers. This is consistent with the results in Fig. 4A showing a larger decrease of the spin majority component of the $d^{\uparrow}_{sm}$ surface state upon laser excitation. Furthermore, the transport of spin-polarized electrons is corroborated by an increase of the spin polarization of the Fe minority spin surface resonance $SR^{\downarrow}_{sm}$ (Fig. 6B and Fig. S5; Supplementary Materials), which we observe superimposed to the demagnetization (decrease of P) of the Fe layer in Fe/Gd.

At first glance, one might expect a spin dependence of the optical excitation in Gd. However, because of spin mixing in Gd, which must be comparable for surface and bulk states, spin-conserving optical transitions cannot lead to an imbalanced depopulation of the occupied surface state.

This should likewise hold for the Gd/Fe bilayer. The Gd $d^{\uparrow}_{sm}$ surface state is derived from the d bulk bands and is a single spin-mixed band, broadened by hybridization. The apparent peak splitting of 80 meV between majority and minority spin components occurs within the width of the $d^{\uparrow}_{sm}$ band. Furthermore, the former is much smaller than the 700-meV exchange splitting of Gd. Because we assume a comparable broadening and apparent splitting for the spin-mixed bulk bands, we do not expect a strong modification of optical matrix elements that could solely explain the sizeable drop of the spin polarization observed for Gd/Fe.

Furthermore, we can exclude sizeable spin-dependent (!) superdiffusive transport in Gd as predicted by Battiato *et al.* (*31*), e.g., for ferromagnetic nickel, because spin-dependent velocities and/or lifetimes should have the same impact on carrier transport and magnetization dynamics in Gd and Gd/Fe. The ultrafast drop of the spin polarization in the $d^{\uparrow}_{sm}$ surface state of the Gd/Fe bilayer occurs within 100 fs. This covers the time scale of both ballistic and superdiffusive transport in the 5-nm-thick Gd film considering typical Fermi and superdiffusive velocities of ~1 to 10 nm/fs (*29*, *31*). Thus, we cannot distinguish between both processes and separate transport from optical excitation. It is the combination of spin transfer from localized surface to delocalized bulk states (OISTR) and the concomitant transport of spins into the Fe layer (spin-polarized current) that drives the drop of the Gd spin polarization in the first 100 fs for Gd/Fe.

The time scale matches as well the increase of the spin polarization in the Fe minority spin resonance $SR^{\downarrow}_{sm}$ of the Fe/Gd bilayer. We do not expect OISTR between the Fe surface resonance and bulk states to drive this increase because the spin-dependent density of the Fe bulk states would strongly favor a depletion of the minority spin component of $SR^{\downarrow}_{sm}$. The superimposed overall decay of the spin polarization is attributed to magnon emission and consistent with (*51*).

We conclude that Fe acts as a spin filter, favoring the transport of Gd majority spins into Fe, where they become minority spins. The Fe film constitutes an efficient absorber of hot electrons. Magneto optical Kerr effect measurements of (epitaxially grown) Co on Cu(001) show that hot electrons excited in the Cu substrate only affect the magnetization dynamics within the first 6 nm of cobalt at the Co/Cu interface (*12*). We confirmed this mean free path studying spin-dependent hot electron lifetimes of Co for Co/Cu(001) (*46*) and found even smaller values of 3 nm for Fe/Cu(001) (*58*). Even shorter mean free paths, albeit for higher kinetic energies of photoelectrons, were reported in (*59*). Contrary, for Gd/W(110), the electrons optically excited to unoccupied Gd bulk states are transported out of the Gd layer into the paramagnetic W(110) substrate independent of their spin. Strong spin-orbit coupling in tungsten will effectively mitigate any spin dependence (*60*). Vice versa, photoexcited electrons in W will be transported into the Gd layer (*60*). The Fermi distribution measured in photoemission

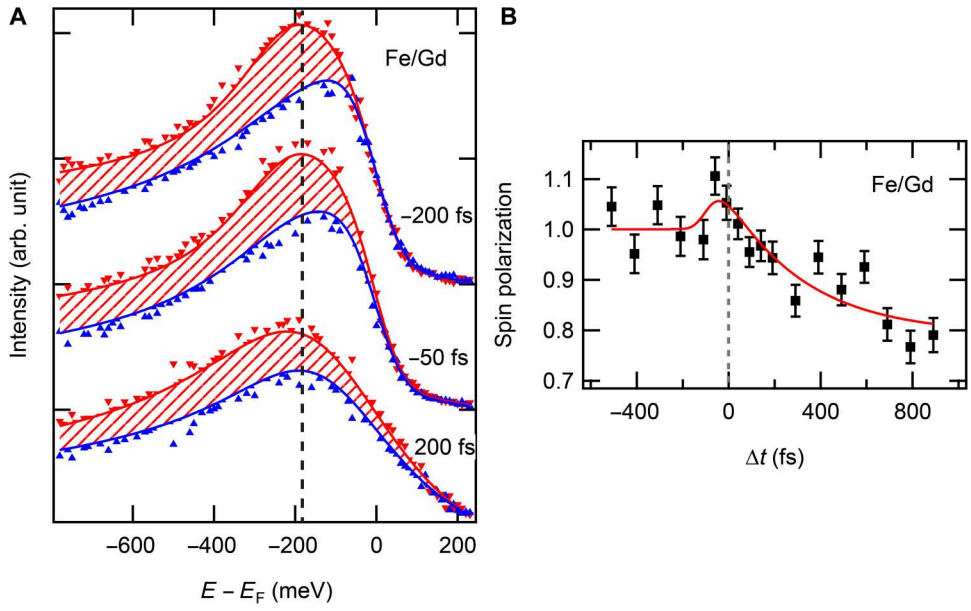

Fig. 6. Spin-resolved spectra of the Fe surface resonance and its transient spin polarization. (**A**) Spin minority (red down-triangle) and spin majority (blue up-triangle) components of the occupied, spin-mixed Fe surface resonance $SR^{\downarrow}_{sm}$ for the reversed Fe/Gd bilayer before (negative delay) and after optical excitation. Note the peak shift between both components induced by the spin-dependent hybridization of Fe and Gd bands. The initial peak position of the minority spin component of the surface resonance is indicated by the dashed line. (**B**) In the Fe/Gd bilayer, the spin polarization of $SR^{\downarrow}_{sm}$ shows an instantaneous increase reflecting the rising edge of the cross-correlation of pump and probe pulses superimposed on the overall decay of *P* upon optical excitation. Error bars represent 1 SD. The solid line is a double-exponential fit (Eq. 2) with rise and decay constants of 50 and 500 fs, convoluted with the 86-fs cross-correlation of pump and probe pulses.

reflects the electron temperature close to the surface of the bilayer. Electrons thermalize via electron-electron scattering within ~200 fs (*61*), which favors exchange scattering and, thus, balance between majority spin and minority spin electrons (*46*). The fact that the electron temperature drops to its initial value for Gd/Fe implies that photoexcited carriers are efficiently transported out of the Gd layer and stopped in the Fe layer. Tallying with this, the electron temperature measured for the reversed Fe/Gd bilayer equilibrates at elevated temperature (see the Supplementary Materials). The time scale of heat transport via phonons is set by phonon velocities (~1 nm/ps), and therefore, the backflow of heat via phonons is considerably slower than the subpicosecond decay of the electron temperature. This explains the different temperatures measured at 2-ps delay for Gd/W and Gd/W/Fe.

We lastly discuss the exceptional dynamics of the surface state binding energy in the Gd/Fe bilayer. Before optical excitation majority and minority spin components of the occupied part of the spin-mixed surface state, $d^{\uparrow}_{sm}$ shows a broadening and apparent peak splitting. E_B of the majority spin component of 180 meV is identical to the binding energy of the surface state on the pure Gd film (which shows no peak splitting). E_B of the minority spin component is lowered to 100 meV. This difference is attributed to the distinct hybridization of Gd 5d and Fe 3d states at the interface, which is, according to ab initio electronic structure calculations, stronger for the minority spin states because, before hybridization, the gap between minority spin Gd 5d and Fe 3d bands is smaller than the gap between the majority spin bands (*62*). Note that this difference in hybridization likewise favors the antiferromagnetic coupling of Gd and Fe layers. Spin mixing or band mirroring is usually assumed to be related to excitation of magnons. In other words, the spin polarization of the bulk and surface valence states, reflecting the magnetic moment, fluctuates in time and space. In our measurement, we average over these fluctuations and observe a reduced spin polarization. In the case of pure Gd, one would expect a broadening in the range of the magnon energies of ~20 meV (*57*). However, in the case of Gd/Fe, an antiparallel/parallel spin alignment is energetically favorable/unfavorable. Therefore, we expect an additional broadening of the band due to spin fluctuations because a band with predominantly majority spin character will have a higher binding energy than a band with predominantly minority spin character. This should likewise lead to a shift of the peak maxima (centers of the band) between majority and minority spin components, which leads to an apparent peak splitting. Furthermore, we find the same apparent peak splitting of ~80 meV not only for the Gd $d^{\uparrow}_{sm}$ surface state but also for the Fe $SR^{\downarrow}_{sm}$ surface resonance in Figs. 1A and 6A, respectively. In line with the antiferromagnetic coupling, the peak order of spin majority and minority components is the reverse for Gd and Fe.

After optical excitation, we observe an overall reduction of the apparent peak splitting between majority and minority spin components. This is explained by the weakening of the antiferromagnetic coupling following the quenching of magnetization and spin polarization in both layers. Nevertheless, for the Gd $d^{\uparrow}_{sm}$ surface state on Gd/Fe, we do observe an unexpected transient increase (!) of the binding energy.

We note that thermal heating leads to the expected decrease of E_B (see the Supplementary Materials, fig. S3C). Because the occupied $d^{\uparrow}_{sm}$ surface state is close below E_F, it is cut by the Fermi level. Thus, the shift to higher binding energy must cause a small repopulation and a concomitant increase of the surface state's magnetic moment.

In (*53*), we have shown for Gd/W(110) that the 5d exchange splitting and the 4f magnetic moments (measured via the linear magnetic dichroism in 4f photoemission) exhibit in the first few picoseconds after optical excitation disparate (!) dynamics with markedly different responses: The exchange splitting drops with a characteristic time of ~700 fs, while the 4f spin order drops with a much slower time constant of ~15 ps. In (*42*) and also confirmed here for the first 2 ps, we observe a similar slow response time of 15 ps of the spin polarization of the Gd $d^{\uparrow}_{sm}$ surface state, while the shift of the binding energy of $d^{\uparrow}_{sm}$ shows again a response time of 600 fs attributed to electron-phonon spin-flip scattering (*42*). These observations suggest that 4f spin system and valence band spin polarization are intimately coupled, while the valence band exchange splitting in Gd can show disparate dynamics. Assuming likewise disparate dynamics of 5d exchange splitting and spin polarization for Gd/Fe, we argue that the drop of the spin polarization of the $d^{\uparrow}_{sm}$ surface state drives its unusual shift to higher binding energy, which partly compensates the former. Because 4f magnetic moment and surface state spin polarization are intimately coupled, we furthermore speculate that the ultrafast reduction of the spin polarization may be accompanied by a reduction of the 4f magnetic moment.

In conclusion, the spin dynamics in an antiferromagnetically coupled Gd/Fe bilayer is distinctly different from the spin dynamics in a single Gd layer epitaxially grown on W(110). Using time- and spin-resolved photoemission spectroscopy, we observe an ultrafast drop of the spin polarization of the spin-mixed Gd $d^{\uparrow}_{sm}$ surface state for the bilayer within 100 fs. This is attributed to efficient spin transport between Gd surface and Fe layer, where the Gd/Fe interface acts as a spin filter favoring the transport of Gd majority spin electrons into Fe. This is confirmed by reverting the bilayer. For Fe/Gd, we observe a transient increase of the minority spin polarization of the Fe $SR^{\downarrow}_{sm}$ surface resonance. Efficient spin transport out of the Gd layer manifests also in the electronic temperature, which decays to its initial value within 1 ps. In contrast, for the pure Gd layer, the spin polarization of the $d^{\uparrow}_{sm}$ surface state stays constant while it shifts to lower binding energy in line with a decrease of the exchange splitting. The electron and lattice subsystems equilibrate at elevated temperature after 1.5 ps. What is more, the antiparallel alignment of Gd and Fe magnetization causes an apparent peak splitting of the spin-mixed surface state. Simultaneously to the ultrafast drop of the spin polarization, we observe an increase of the binding energy of the Gd surface state, which must partly compensate the former. This is again a manifestation of the disparate dynamics of exchange splitting and spin polarization in Gd (*53*), which we assigned to the intimate coupling between spin polarization and 4f magnetic moment (*42*).

Our results provide clear evidence that magnetization dynamics in the Gd/Fe bilayer can be driven by spin transport. We see distinct signatures in the spin-dependent electronic structure that allow us to gain microscopic insights into ultrafast spin dynamics. These findings are of general importance for the understanding of magnetization switching in ferrimagnetic Gd-Fe compounds.

MATERIALS AND METHODS

Experimental setup

In the time-resolved photoemission experiment, we apply the fundamental of a Ti:sapphire regenerative amplifier (RegA, Coherent) with a photon energy of 1.57 eV as pump pulse. The repetition rate of the laser system is set to 300 kHz. The absorbed pump fluence was 2.3 ± 0.5 mJ/cm^2. The time-delayed ultraviolet probe pulse with 6.3-eV photon energy is obtained by consecutive second, third, and fourth harmonic generation. The cross-correlation of pump and probe beams was 86 fs (*42*). (Multiphoton)-photoemission is usually enhanced/suppressed when the electric field vector is perpendicularly/parallelly aligned to the surface plane. Accordingly, the pump pulses were s-polarized to avoid space charge effects caused by multiphoton photoemission, and the probe pulses were p-polarized to enhance the photoemission yield. Pump and probe light are collinearly incident on the sample at an angle of 45° with respect to the sample normal (Gd [1000]-direction). Photoelectrons are detected in normal emission after a cylindrical sector analyzer (CSA 300, Focus) with energy and angular resolutions of 65 meV and 2.5°, respectively. For spin-resolved measurements, an exchange-scattering target is inserted into the electron trajectory. As scattering target, we use an in-plane magnetized six-monolayer Fe film epitaxially grown on W(100) and passivated with an oxygen p(1x1) superstructure (*63*). The highest figure of merit of the spin detector (Sherman function $S = 0.24$) is obtained for a scattering energy of 6 eV. The spin polarization is determined by reverting the magnetization of the Fe scattering target. The pressure during measurements was 2×10^{-11} mbar. The sample temperature was 100 K. Both samples were magnetized in the direction along the in-plane easy axis of the Fe layer (M ∥ $[1\bar{1}0]$-direction), and the spin polarization of the photoelectrons is measured in remanence with respect to this direction. For Gd, this corresponds to the $[\bar{1}100]$ direction.

Sample preparation

Gd single layer and Gd/Fe and Fe/Gd bilayers were prepared by molecular beam epitaxy at a pressure of 1×10^{-10} mbar during sample growth. For the pure Gd film with a thickness of 5 nm, Gd was deposited directly on the (110) surface of a tungsten (W) single crystal and was subsequently annealed at 600 K for 600 s. For the Gd/Fe bilayer, Fe was first deposited on the W(110) crystal with a thickness of 3 nm, followed by Gd evaporation of 5 nm. The bilayer system was also annealed at 600 K for 600 s. For the Fe/Gd bilayer, Gd was first deposited on the W(110) crystal with a thickness of 5 nm followed by Fe evaporation of 3 nm. The bilayer system was annealed at 550 K for 600 s. Thin-film quality was controlled by monitoring both low-energy electron diffraction (LEED) patterns and the Gd and Fe surface state. After the annealing procedure, both Gd films show sharp LEED patterns of the hexagonal close-packed Gd(0001) surface. The Fe film shows the bcc pattern of Fe(110), although much fainter compared to pure Fe on W(110) (see the Supplementary Materials).

Data analysis

To determine the spin- and time-dependent binding energy E_B of the surface state in Fig. 3, we fitted each spin-resolved spectrum in Fig. 2 with a single Lorentzian function superimposed on a linear

background, which is cut by the Fermi distribution

$$I = y_0 + \left\{ \left[a + b \cdot E + \frac{A \cdot (\Gamma/2)^2}{4 \cdot (E - E_B)^2 + (\Gamma/2)^2} \right] \cdot f(E, T_e) \right\} \otimes g(E) \quad (1)$$

The fit function was convolved with a Gaussian $g(E)$ of fixed 100-meV full width at half maximum (FWHM) that represents the instrumental resolution determined by the UV laser pulse and the electron analyzer. The constant offset y_0 accounts for dark counts of the channeltron, and $a + b{\cdot}E$ is a linear background describing secondary electrons and the increasing density of states toward E_F (*64*). The Lorentzian resembles the spectral function of the surface state majority and minority spin components I_{maj} and I_{min} with amplitude A and linewidth Γ. $f(E, T_e)$ is the Fermi function depending on the electron temperature T_e.

The spectral intensity I_{maj} and I_{min} and spin polarization P in Fig. 4 were evaluated by integrating the spin-resolved spectra of Fig. 2 over an energy range from $E - E_F = -600$ to 100 meV. We describe the dynamics of the binding energy E_B, spectral intensity I_{maj} and I_{min}, spin polarization P, and electron temperature T_e by a double exponential decay convolved with a Gaussian $g(t)$:

$$\Delta I(t) = g(t) \otimes \left[1 - H(t - t_0) \cdot \left(A_1 \left\{ 1 - \exp\left[\frac{-(t - t_0)}{\tau_1} \right] \right\} \cdot \exp\left[\frac{-(t - t_0)}{\tau_2} \right] + A_2 \left\{ 1 - \exp\left[\frac{-(t - t_0)}{\tau_2} \right] \right\} \right) \right] \quad (2)$$

Here, A_1 and A_2 represents the decay amplitudes with decay times τ_1 and τ_2. t_0 refers to zero delay between pump and probe pulses. The FWHM of the Gaussian corresponds to the cross-correlation of pump and probe pulses of 86 fs. $H(t)$ is the Heaviside function.

Supplementary Materials

This PDF file includes:

Supplementary Text
Figs. S1 to S5
References

REFERENCES AND NOTES

1. A. Kirilyuk, A. V. Kimel, T. Rasing, Ultrafast optical manipulation of magnetic order. *Rev. Mod. Phys.* **82**, 2731–2784 (2010).
2. E. Beaurepaire, J. C. Merle, A. Daunois, J. Y. Bigot, Ultrafast spin dynamics in ferromagnetic nickel. *Phys. Rev. Lett.* **76**, 4250–4253 (1996).
3. L. C. Bassett, F. J. Heremans, D. J. Christle, C. G. Yale, G. Burkard, B. B. Buckley, D. D. Awschalom, Ultrafast optical control of orbital and spin dynamics in a solid-state defect. *Science* **345**, 1333–1337 (2014).
4. C. D. Stanciu, F. Hansteen, A. V. Kimel, A. Kirilyuk, A. Tsukamoto, A. Itoh, T. Rasing, All-optical magnetic recording with circularly polarized light. *Phys. Rev. Lett.* **99**, 047601 (2007).
5. S. R. Tauchert, M. Volkov, D. Ehberger, D. Kazenwadel, M. Evers, H. Lange, A. Donges, A. Book, W. Kreuzpaintner, U. Nowak, P. Baum, Polarized phonons carry angular momentum in ultrafast demagnetization. *Nature* **602**, 73–77 (2022).
6. M. Hofherr, S. Häuser, J. K. Dewhurst, P. Tengdin, S. Sakshath, H. T. Nembach, S. T. Weber, J. M. Shaw, T. J. Silva, H. C. Kapteyn, M. Cinchetti, B. Rethfeld, M. M. Murnane, D. Steil, B. Stadtmüller, S. Sharma, M. Aeschlimann, S. Mathias, Ultrafast optically induced spin transfer in ferromagnetic alloys. *Sci. Adv.* **6**, eaay8717 (2020).
7. P. Tengdin, C. Gentry, A. Blonsky, D. Zusin, M. Gerrity, L. Hellbrück, M. Hofherr, J. Shaw, Y. Kvashnin, E. K. Delczeg-Czirjak, M. Arora, H. Nembach, T. J. Silva, S. Mathias, M. Aeschlimann, H. C. Kapteyn, D. Thonig, K. Koumpouras, O. Eriksson, M. M. Murnane, Direct light-induced spin transfer between different elements in a spintronic Heusler material via femtosecond laser excitation. *Sci. Adv.* **6**, eaaz1100 (2020).
8. V. Shokeen, M. Sanchez Piaia, J. Y. Bigot, T. Müller, P. Elliott, J. K. Dewhurst, S. Sharma, E. K. U. Gross, Spin flips versus spin transport in nonthermal electrons excited by ultrashort optical pulses in transition metals. *Phys. Rev. Lett.* **119**, 107203 (2017).
9. C. Dornes, Y. Acremann, M. Savoini, M. Kubli, M. J. Neugebauer, E. Abreu, L. Huber, G. Lantz, C. A. F. Vaz, H. Lemke, E. M. Bothschafter, M. Porer, V. Esposito, L. Rettig, M. Buzzi, A. Alberca, Y. W. Windsor, P. Beaud, U. Staub, D. Zhu, S. Song, J. M. Glownia, S. L. Johnson, The ultrafast Einstein-de Haas effect. *Nature* **565**, 209–212 (2019).
10. M. Hennecke, I. Radu, R. Abrudan, T. Kachel, K. Holldack, R. Mitzner, A. Tsukamoto, S. Eisebitt, Angular momentum flow during ultrafast demagnetization of a ferrimagnet. *Phys. Rev. Lett.* **122**, 157202 (2019).
11. N. Bergeard, M. Hehn, S. Mangin, G. Lengaigne, F. Montaigne, M. L. M. Lalieu, B. Koopmans, G. Malinowski, Hot-electron-induced ultrafast demagnetization in Co/Pt multilayers. *Phys. Rev. Lett.* **117**, 147203 (2016).
12. J. Wieczorek, A. Eschenlohr, B. Weidtmann, M. Rösner, N. Bergeard, A. Tarasevitch, T. O. Wehling, U. Bovensiepen, Separation of ultrafast spin currents and spin-flip scattering in Co/Cu(001) driven by femtosecond laser excitation employing the complex magneto-optical Kerr effect. *Phys. Rev. B* **92**, 174410 (2015).
13. Y. Beyazit, J. Beckord, P. Zhou, J. P. Meyburg, F. Kühne, D. Diesing, M. Ligges, U. Bovensiepen, Local and nonlocal electron dynamics of Au/Fe/MgO(001) heterostructures analyzed by time-resolved two-photon photoemission spectroscopy. *Phys. Rev. Lett.* **125**, 076803 (2020).
14. D. Steil, J. Walowski, F. Gerhard, T. Kiessling, D. Ebke, A. Thomas, T. Kubota, M. Oogane, Y. Ando, J. Otto, A. Mann, M. Hofherr, P. Elliott, J. K. Dewhurst, G. Reiss, L. Molenkamp, M. Aeschlimann, M. Cinchetti, M. Münzenberg, S. Sharma, S. Mathias, Efficiency of ultrafast optically induced spin transfer in Heusler compounds. *Phys. Rev. Res.* **2**, 023199 (2020).
15. F. Willems, C. von Korff Schmising, C. Strüber, D. Schick, D. W. Engel, J. K. Dewhurst, P. Elliott, S. Sharma, S. Eisebitt, Optical inter-site spin transfer probed by energy and spin-resolved transient absorption spectroscopy. *Nat. Commun.* **11**, 871 (2020).
16. F. Siegrist, J. A. Gessner, M. Ossiander, C. Denker, Y.-P. Chang, M. C. Schröder, A. Guggenmos, Y. Cui, J. Walowski, U. Martens, J. K. Dewhurst, U. Kleineberg, M. Münzenberg, S. Sharma, M. Schultze, Light-wave dynamic control of magnetism. *Nature* **571**, 240–244 (2019).
17. J. K. Dewhurst, P. Elliott, S. Shallcross, E. K. U. Gross, S. Sharma, Laser-induced intersite spin transfer. *Nano Lett.* **18**, 1842–1848 (2018).
18. B. Frietsch, A. Donges, R. Carley, M. Teichmann, J. Bowlan, K. Döbrich, K. Carva, D. Legut, P. M. Oppeneer, U. Nowak, M. Weinelt, The role of ultrafast magnon generation in the magnetization dynamics of rare-earth metals. *Sci. Adv.* **6**, eabb1601 (2020).
19. A. B. Schmidt, M. Pickel, M. Donath, P. Buczek, A. Ernst, V. P. Zhukov, P. M. Echenique, L. M. Sandratskii, E. V. Chulkov, M. Weinelt, Ultrafast magnon generation in an Fe Film on Cu(100). *Phys. Rev. Lett.* **105**, 197401 (2010).
20. B. Koopmans, G. Malinowski, F. Dalla Longa, D. Steiauf, M. Fähnle, T. Roth, M. Cinchetti, M. Aeschlimann, Explaining the paradoxical diversity of ultrafast laser-induced demagnetization. *Nat. Mater.* **9**, 259–265 (2010).
21. M. Krauß, T. Roth, S. Alebrand, D. Steil, M. Cinchetti, M. Aeschlimann, H. C. Schneider, Ultrafast demagnetization of ferromagnetic transition metals: The role of the Coulomb interaction. *Phys. Rev. B* **80**, 180407 (2009).
22. S. Iihama, Q. Remy, J. Igarashi, G. Malinowski, M. Hehn, S. Mangin, Spin-transport mediated single-shot all-optical magnetization switching of metallic films. *J. Phys. Soc. Jpn.* **90**, 081009 (2021).
23. K. Bühlmann, G. Saerens, A. Vaterlaus, Y. Acremann, Detection of femtosecond spin injection into a thin gold layer by time and spin resolved photoemission. *Sci. Rep.* **10**, 12632 (2020).
24. S. Iihama, Y. Xu, M. Deb, G. Malinowski, M. Hehn, J. Gorchon, E. E. Fullerton, S. Mangin, Single-shot multi-level all-optical magnetization switching mediated by spin transport. *Adv. Mater.* **30**, 1804004 (2018).
25. M. Hofherr, P. Maldonado, O. Schmitt, M. Berritta, U. Bierbrauer, S. Sadashivaiah, A. J. Schellekens, B. Koopmans, D. Steil, M. Cinchetti, B. Stadtmüller, P. M. Oppeneer, S. Mathias, M. Aeschlimann, Speed and efficiency of femtosecond spin current injection into a nonmagnetic material. *Phys. Rev. B* **96**, 100403 (2017).
26. A. Alekhin, I. Razdolski, N. Ilin, J. P. Meyburg, D. Diesing, V. Roddatis, I. Rungger, M. Stamenova, S. Sanvito, U. Bovensiepen, A. Melnikov, Femtosecond spin current pulses generated by the nonthermal spin-dependent seebeck effect and interacting with ferromagnets in spin valves. *Phys. Rev. Lett.* **119**, 017202 (2017).
27. A. Eschenlohr, M. Battiato, P. Maldonado, N. Pontius, T. Kachel, K. Holldack, R. Mitzner, A. Föhlisch, P. M. Oppeneer, C. Stamm, Ultrafast spin transport as key to femtosecond demagnetization. *Nat. Mater.* **12**, 332–336 (2013).

28. D. Rudolf, C. La-o-vorakiat, M. Battiato, R. Adam, J. M. Shaw, E. Turgut, P. Maldonado, S. Mathias, P. Grychtol, H. T. Nembach, T. J. Silva, M. Aeschlimann, H. C. Kapteyn, M. M. Murnane, C. M. Schneider, P. M. Oppeneer, Ultrafast magnetization enhancement in metallic multilayers driven by superdiffusive spin current. *Nat. Commun.* **3**, 1037 (2012).
29. M. Battiato, K. Carva, P. M. Oppeneer, Theory of laser-induced ultrafast superdiffusive spin transport in layered heterostructures. *Phys. Rev. B* **86**, 024404 (2012).
30. A. Melnikov, I. Razdolski, T. O. Wehling, E. T. Papaioannou, V. Roddatis, P. Fumagalli, O. Aktsipetrov, A. I. Lichtenstein, U. Bovensiepen, Ultrafast transport of laser-excited spin-polarized carriers in Au/Fe/MgO(001). *Phys. Rev. Lett.* **107**, 076601 (2011).
31. M. Battiato, K. Carva, P. M. Oppeneer, Superdiffusive spin transport as a mechanism of ultrafast demagnetization. *Phys. Rev. Lett.* **105**, 027203 (2010).
32. G. Malinowski, F. Dalla Longa, J. H. H. Rietjens, P. V. Paluskar, R. Huijink, H. J. M. Swagten, B. Koopmans, Control of speed and efficiency of ultrafast demagnetization by direct transfer of spin angular momentum. *Nat. Phys.* **4**, 855–858 (2008).
33. I. Razdolski, A. Alekhin, N. Ilin, J. P. Meyburg, V. Roddatis, D. Diesing, U. Bovensiepen, A. Melnikov, Nanoscale interface confinement of ultrafast spin transfer torque driving non-uniform spin dynamics. *Nat. Commun.* **8**, 15007 (2017).
34. A. J. Schellekens, K. C. Kuiper, R. R. J. C. de Wit, B. Koopmans, Ultrafast spin-transfer torque driven by femtosecond pulsed-laser excitation. *Nat. Commun.* **5**, 4333 (2014).
35. T. Lichtenberg, M. Beens, M. H. Jansen, B. Koopmans, R. A. Duine, Probing optically induced spin currents using terahertz spin waves in noncollinear magnetic bilayers. *Phys. Rev. B* **105**, 144416 (2022).
36. R. Rouzegar, L. Brandt, L. Nádvorník, D. A. Reiss, A. L. Chekhov, O. Gueckstock, C. In, M. Wolf, T. S. Seifert, P. W. Brouwer, G. Woltersdorf, T. Kampfrath, Laser-induced terahertz spin transport in magnetic nanostructures arises from the same force as ultrafast demagnetization. *Phys. Rev. B* **106**, 144427 (2022).
37. M. Beens, R. A. Duine, B. Koopmans, Modeling ultrafast demagnetization and spin transport: The interplay of spin-polarized electrons and thermal magnons. *Phys. Rev. B* **105**, 144420 (2022).
38. M. Beens, R. A. Duine, B. Koopmans, *s*–*d* Model for local and nonlocal spin dynamics in laser-excited magnetic heterostructures. *Phys. Rev. B* **102**, 054442 (2020).
39. E. G. Tveten, A. Brataas, Y. Tserkovnyak, Electron-magnon scattering in magnetic heterostructures far out of equilibrium. *Phys. Rev. B* **92**, 180412 (2015).
40. G.-M. Choi, B.-C. Min, K.-J. Lee, D. G. Cahill, Spin current generated by thermally driven ultrafast demagnetization. *Nat. Commun.* **5**, 4334 (2014).
41. I.-H. Shin, B.-C. Min, B.-K. Ju, G.-M. Choi, Ultrafast spin current generated by electron–magnon scattering in bulk of ferromagnets. *Jpn. J. Appl. Phys.* **57**, 090307 (2018).
42. B. Andres, M. Christ, C. Gahl, M. Wietstruk, M. Weinelt, J. Kirschner, Separating exchange splitting from spin mixing in gadolinium by femtosecond laser excitation. *Phys. Rev. Lett.* **115**, 207404 (2015).
43. Y. L. W. van Hees, P. van de Meugheuvel, B. Koopmans, R. Lavrijsen, Deterministic all-optical magnetization writing facilitated by non-local transfer of spin angular momentum. *Nat. Commun.* **11**, 3835 (2020).
44. A. V. Kimel, M. Li, Writing magnetic memory with ultrashort light pulses. *Nat. Rev. Mater.* **4**, 189–200 (2019).
45. S. Eich, M. Plötzing, M. Rollinger, S. Emmerich, R. Adam, C. Chen, H. C. Kapteyn, M. M. Murnane, L. Plucinski, D. Steil, B. Stadtmüller, M. Cinchetti, M. Aeschlimann, C. M. Schneider, S. Mathias, Band structure evolution during the ultrafast ferromagnetic-paramagnetic phase transition in cobalt. *Sci. Adv.* **3**, e1602094 (2017).
46. A. Goris, K. M. Döbrich, I. Panzer, A. B. Schmidt, M. Donath, M. Weinelt, Role of spin-flip exchange scattering for hot-electron lifetimes in cobalt. *Phys. Rev. Lett.* **107**, 026601 (2011).
47. M. Lisowski, P. A. Loukakos, A. Melnikov, I. Radu, L. Ungureanu, M. Wolf, U. Bovensiepen, Femtosecond electron and spin dynamics in Gd(0001) studied by time-resolved photoemission and magneto-optics. *Phys. Rev. Lett.* **95**, 137402 (2005).
48. M. Bode, M. Getzlaff, A. Kubetzka, R. Pascal, O. Pietzsch, R. Wiesendanger, Temperature-dependent exchange splitting of a surface state on a local-moment magnet: Tb(0001). *Phys. Rev. Lett.* **83**, 3017–3020 (1999).
49. K. Maiti, M. C. Malagoli, A. Dallmeyer, C. Carbone, Finite temperature magnetism in Gd: Evidence against a stoner behavior. *Phys. Rev. Lett.* **88**, 167205 (2002).
50. B. Andres, M. Weinelt, H. Ebert, J. Braun, A. Aperis, P. M. Oppeneer, Strong momentum-dependent electron–magnon renormalization of a surface resonance on iron. *Appl. Phys. Lett.* **120**, 202404 (2022).
51. R. Gort, K. Bühlmann, S. Däster, G. Salvatella, N. Hartmann, Y. Zemp, S. Holenstein, C. Stieger, A. Fognini, T. U. Michlmayr, T. Bähler, A. Vaterlaus, Y. Acremann, Early stages of ultrafast spin dynamics in a 3D ferromagnet. *Phys. Rev. Lett.* **121**, 087206 (2018).
52. R. Carley, K. Döbrich, B. Frietsch, C. Gahl, M. Teichmann, O. Schwarzkopf, P. Wernet, M. Weinelt, Femtosecond laser excitation drives ferromagnetic gadolinium out of magnetic equilibrium. *Phys. Rev. Lett.* **109**, 057401 (2012).
53. B. Frietsch, J. Bowlan, R. Carley, M. Teichmann, S. Wienholdt, D. Hinzke, U. Nowak, K. Carva, P. M. Oppeneer, M. Weinelt, Disparate ultrafast dynamics of itinerant and localized magnetic moments in gadolinium metal. *Nat. Commun.* **6**, 8262 (2015).
54. A. Melnikov, I. Radu, U. Bovensiepen, O. Krupin, K. Starke, E. Matthias, M. Wolf, Coherent optical phonons and parametrically coupled magnons induced by femtosecond laser excitation of the Gd(0001) surface. *Phys. Rev. Lett.* **91**, 227403 (2003).
55. E. Carpene, E. Mancini, C. Dallera, M. Brenna, E. Puppin, S. De Silvestri, Dynamics of electron-magnon interaction and ultrafast demagnetization in thin iron films. *Phys. Rev. B* **78**, 174422 (2008).
56. M. Bauer, A. Marienfeld, M. Aeschlimann, Hot electron lifetimes in metals probed by time-resolved two-photon photoemission. *Prog. Surf. Sci.* **90**, 319–376 (2015).
57. B. Liu, H. Xiao, G. Siemann, J. Weber, B. Andres, W. Bronsch, P. M. Oppeneer, M. Weinelt, Signature of magnon polarons in electron relaxation on terbium revealed by comparison with gadolinium. *Phys. Rev. B* **104**, 024434 (2021).
58. A. Goris, thesis (2010).
59. G. Schönhense, H. C. Siegmann, Transmission of electrons through ferromagnetic material and applications to detection of electron spin polarization. *Ann. Phys.* **505**, 465–474 (1993).
60. E. Turgut, C. La-o-vorakiat, J. M. Shaw, P. Grychtol, H. T. Nembach, D. Rudolf, R. Adam, M. Aeschlimann, C. M. Schneider, T. J. Silva, M. M. Murnane, H. C. Kapteyn, S. Mathias, Controlling the competition between optically induced ultrafast spin-flip scattering and spin transport in magnetic multilayers. *Phys. Rev. Lett.* **110**, 197201 (2013).
61. U. Bovensiepen, Coherent and incoherent excitations of the Gd(0001) surface on ultrafast timescales. *J. Phys. Condens. Matter* **19**, 083201 (2007).
62. M. S. S. Brooks, T. Gasche, S. Auluck, L. Nordström, L. Severin, J. Trygg, B. Johansson, *Ab initio* calculation of molecular field interactions in rare-earth transition-metal intermetallics (invited). *J. Appl. Phys.* **70**, 5972 (1998).
63. A. Winkelmann, D. Hartung, H. Engelhard, C. T. Chiang, J. Kirschner, High efficiency electron spin polarization analyzer based on exchange scattering at Fe/W(001). *Rev. Sci. Instrum.* **79**, 083303 (2008).
64. E. Weschke, C. Schüßler-Langeheine, R. Meier, A. V. Fedorov, K. Starke, F. Hübinger, G. Kaindl, Temperature dependence of the exchange splitting of the surface state on Gd(0001): Evidence against spin-mixing behavior. *Phys. Rev. Lett.* **77**, 3415–3418 (1996).
65. J. L. Prieto, B. B. van Aken, G. Burnell, C. Bell, J. E. Evetts, N. Mathur, M. G. Blamire, Transport properties of sharp antiferromagnetic boundaries in Gd/Fe multilayers. *Phys. Rev. B* **69**, 054436 (2004).
66. M. Romera, J. Grollier, S. Collin, T. Devolder, V. Cros, M. Muñoz, J. L. Prieto, Enhanced stability in spin transfer nanopillars due to a Fe/Gd/Fe trilayer. *Appl. Phys. Lett.* **103**, 122404 (2013).
67. N. I. Medvedeva, D. Van Aken, J. E. Medvedeva, Magnetism in bcc and fcc Fe with carbon and manganese. *J. Phys. Condens. Matter* **22**, 316002 (2010).
68. J. Hintermayr, A. Ullrich, M. Albrecht, Structure and magnetic properties of ferrimagnetic $[Gd/Fe]_n$ multilayer and Gd_xFe_{100-x} thin films. *AIP Adv.* **11**, 095214 (2021).
69. M. L. M. Lalieu, M. J. G. Peeters, S. R. R. Haenen, R. Lavrijsen, B. Koopmans, Deterministic all-optical switching of synthetic ferrimagnets using single femtosecond laser pulses. *Phys. Rev. B* **96**, 220411 (2017).

Acknowledgments

Funding: This project was supported by Deutsche Forschungsgemeinschaft and the Collaborative Research Center TRR 227 on Ultrafast Spin Dynamics, project A1. H.X. is indebted to the China Scholarship Council for financial support. **Author contributions:** The design of the study was carried out by M.W. B.L. and H.X. performed the experiment and data analysis. The paper was written with contributions from all authors. **Competing interests:** The authors declare that they have no competing interests. **Data and materials availability:** All data needed to evaluate the conclusions in the paper are present in the paper and/or the Supplementary Materials. The photoemission data used for the presented analysis are publicly available under 10.5281/zenodo.7553188.

Submitted 20 July 2022
Accepted 13 April 2023
Published 17 May 2023
10.1126/sciadv.ade0286

ScienceAdvances

Microscopic insights to spin transport–driven ultrafast magnetization dynamics in a Gd/Fe bilayer

Bo Liu, Huijuan Xiao, and Martin Weinelt

Sci. Adv., **9** (20), eade0286.
DOI: 10.1126/sciadv.ade0286

Science Advances (ISSN) is published by the American Association for the Advancement of Science. 1200 New York Avenue NW, Washington, DC 20005. The title *Science Advances* is a registered trademark of AAAS.